

Evidence from Galactic Cosmic Rays That the Sun Has Likely Entered A Secular Minimum in Solar Activity

F. Rahmanifard^{1,2}, A. P. Jordan^{1,2}, W. C. de Wet^{1,2}, N. A. Schwadron^{1,2}, J. K. Wilson^{1,2}, M. J. Owens³, H. E. Spence^{1,2}, P. Riley⁴

⁵¹Space Science Center, University of New Hampshire, Durham, NH, USA

⁶²Solar System Exploration Research Virtual Institute, NASA Ames Research Center, Moffett Field, CA,

USA

⁷³Space and Atmospheric Electricity Group, Department of Meteorology, University of Reading, Reading,

UK

⁹¹⁰³Predictive Science, San Diego, CA, USA

Key Points:

- Trends observed in the modulation of GCRs suggest that the Sun might be in a secular minimum
- The next two cycles will probably be weaker than average
- Cycle 25 will be as weak as or weaker than cycle 24

16 **Abstract**

17 Since the beginning of the space age, the Sun has been in a multi-cycle period of elevated
 18 activity (secular maximum). This secular maximum is the longest in the last 9300 years.
 19 Since the end of solar cycle 21 (SC21), however, the Sun has shown a decline in over-
 20 all activity, which has remarkably increased the fluxes of galactic cosmic rays (GCRs).
 21 Here, we investigate the correlation between the modulation of GCRs, the heliospheric
 22 magnetic field, and solar wind speed for the last 24 solar cycles to find trends that can
 23 potentially be used to predict future solar activity. Specifically, we develop a tool for pre-
 24 dicting future magnetic field intensity, based on the hysteresis in the GCR variation, dur-
 25 ing the last phases of the current cycle. This method estimates that SC25 will be as weak
 26 as or weaker than SC24. This would mean that the Sun has likely entered a secular min-
 27 imum, which, according to historical records, should last for another two cycles (SC25
 28 and SC26).

29 **Plain Language Summary**

30 We investigated the correlation between the modulation of galactic cosmic rays (GCRs)
 31 and solar wind parameters to find trends that could be used in predicting future solar
 32 activity. Using this method, we estimate that SC25 will be as weak as or weaker than
 33 SC24. Furthermore, these trends suggest that the Sun might be in a secular minimum.

34 **1 Introduction**

35 Both sunspot numbers (SSN) and the heliospheric magnetic field (HMF) show ap-
 36 proximately 11-year cycles that superpose longer-term quasi-periodic variations, called
 37 secular variations (for more information on solar cycles refer to Hathaway, 2010). Some
 38 of the more prominent secular variations are three grand minima: the Wolf (years 1280-
 39 1350), Maunder (years 1645-1710), and Dalton minima (years 1790-1830, solar cycles 6-
 40 8). In addition, the space age has coincided with the longest grand maximum in 9300
 41 years (Abreu et al., 2008). But the duration of previous maxima and the quasi-periodic
 42 recurrence of these secular variations suggests that this grand maximum is ending, and
 43 the Sun is entering a possible grand minimum—a modern minimum.

44 While the 11-year solar cycles have been known for over a century, the physics be-
 45 hind it is not fully agreed-upon (Charbonneau, 2010). Variations of the solar magnetic
 46 field can be qualitatively described based on the oscillatory exchange of energy between
 47 poloidal and toroidal solar magnetic field components as a driving force for solar cycles.
 48 In this model, the toroidal magnetic field is generated by buoyant upwelling within the
 49 convective zone, which is itself created by the differential rotation of the Sun stretching
 50 the large-scale poloidal component and appears as bipolar magnetic regions (BMRs) on
 51 the Sun’s surface. The effect of Coriolis force on the rising toroidal magnetic flux tubes
 52 tilts these BMRs, and turbulent convection further leads to a dispersion around the mean
 53 tilt. The poloidal component of the solar magnetic field and the resulting active regions
 54 reach their maximum during solar maximum. A poloidal dipolar field, on the other hand,
 55 is created by the shift of energy from the toroidal field to the poloidal field due to the
 56 dispersion and decay of the BMRs via surface flux transport processes during the declin-
 57 ing phase of the solar cycle (Babcock, 1961; Leighton, 1969; Bhowmik & Nandy, 2018).
 58 The large-scale solar magnetic field that is tied to the solar activity cycles as described
 59 above governs the coronal conditions and plays a role in balancing the heliospheric open
 60 flux and the resulting HMF (see e.g., Pal et al., 2020; Schwadron et al., 2010).

61 Many attempts have been made to understand the cause of the longer-term solar
 62 variations. These variations dictate the amplitude of the solar cycles (Lockwood et al.,
 63 1999; Lockwood, 2001; Vaquero, 2016; Usoskin, 2013; Hathaway, 2010; Passos et al., 2014;
 64 Hazra et al., 2014; Weiss & Tobias, 2016; Hazra & Nandy, 2019) and thus affect space

65 weather. As we are resuming human deep space explorations, there is an ever-growing
 66 need to investigate the possibility of entering a deep secular minimum in the coming decades.

67 Radiation from galactic cosmic rays (GCRs) is the main source of concern for crewed
 68 space missions. GCRs are energetic particles, consisting of protons, heavier ions, and a
 69 small fraction of electrons, which enter the heliosphere from the outer space. More than
 70 90% of the GCRs are deflected at the interface between the heliosphere and the inter-
 71 stellar medium by the slowed solar wind. The residual GCRs that enter the heliosphere
 72 are modulated by the HMF. The flux of GCRs, which is inversely-correlated with the
 73 HMF and solar activity (Usoskin, 2013; Schwadron et al., 2014), reaches its maximum
 74 during solar minimum, when the HMF is too weak to modulate GCRs effectively and
 75 vice versa. Their flux can be used to monitor variations of the solar activity, and thus
 76 ^{14}C and ^{10}Be radioisotopes, which are produced by the reaction of GCRs with the Earth's
 77 upper atmosphere, can provide a record of solar activity back to 10,000 years ago (Beer
 78 et al., 2011). The modulation of GCRs represents a response to the solar wind and the
 79 solar magnetic field over the scale of the entire heliosphere. GCR evolution, therefore,
 80 can uniquely reveal some of the trends we might not be able to see otherwise.

81 In a series of papers Lockwood (2010), Owens et al. (2011), and Barnard et al. (2011)
 82 investigated the statistical likelihood of a secular minimum, in particular, a Maunder-
 83 like grand minimum. They performed a superposed epoch analysis of the modulation
 84 parameter at the end of the previous grand solar maxima in the last 9300 years based
 85 on the composite reconstruction of the modulation parameter from Steinhilber et al. (2008).
 86 On the basis of past variations, the probability of a Maunder-like grand minimum in the
 87 coming 50 years was estimated to be around 1 in 12. Furthermore, Owens et al. (2017)
 88 created a data set for solar wind parameters dating back to 1617. They specifically in-
 89 vestigated the Maunder minimum conditions to find the most probable coronal magnetic
 90 field configuration for this period (See Riley et al., 2015) so it could be used for any past
 91 or future grand minima.

92 Many researchers have attempted to predict the amplitude of the past four solar
 93 cycles (SC), 21-24 (1976-2020), using various methods (for a list of the models predict-
 94 ing SC24 and SC25, see Pesnell, 2012, 2016; Nandy, 2021, and the references therein).
 95 Pesnell (2016) concluded that more advanced models based on the solar magnetic field
 96 data are required to provide more reliable forecasts; predictions for SC24 showed a wide
 97 range of predicted amplitudes, proving that we are far from a consensus. Nandy (2021)
 98 argued that while there is no consensus on predicting the strength of SC25 among all
 99 existing studies, physics-based predictions have converged as a result of new insights of
 100 the solar dynamo.

101 Among the models investigated by Pesnell (2016); Nandy (2021), the most success-
 102 ful ones are based on the amplitude of the Sun's polar field (<http://wso.stanford.edu/Polar.html>)
 103 at previous solar minimum. These models predict a SC25 slightly weaker than SC24 (for
 104 example, Upton & Hathaway, 2018; Wang, 2017; Jiang et al., 2018). However, there are
 105 a few studies (based on the same methods) predicting SC25 to be somewhat more ac-
 106 tive than, although still comparable to the current cycle, for example, R. H. Cameron
 107 et al. (2016) and Bhowmik and Nandy (2018). Bhowmik and Nandy (2018) used mod-
 108 els for the evolution of the Sun's surface and interior magnetic field and performed sim-
 109 ulations of solar activity based on over a century of data. They provide a methodology
 110 that extends the prediction window to a decade (rather than the previous cycle minima).

111 McIntosh et al. (2020) and Leamon et al. (2020) have developed a methodology based
 112 on McIntosh et al. (2019) to find the terminator events indicative of the end of a cycle
 113 at the solar equator and the onset of a new cycle at mid-latitudes. Based on these ter-
 114 minators, McIntosh et al. (2020) and Leamon et al. (2020) predicted the onset of SC25
 115 to be May 2020 (-1.5, +4 months) and that SC25 will be stronger than SC23 and SC24,
 116 which is in contrast with the predictions from the studies based on the amplitude of the

117 Sun's polar field at solar minimum. In their analysis, they used activity bands that can-
 118 cel out one another between the different polarization of two consecutive cycles when they
 119 co-exist. These activity bands explain why a prolonged solar minimum results in a weak
 120 next cycle. The solar Cycle 25 Prediction Panel (<https://www.weather.gov/news/190504-sun-activity-in-solar-cycle>) has gathered all these studies to predict the next cycle will
 121 peak at 95 to 130 averaged daily sunspot number. This prediction is most similar to the
 122 Gleissberg period (SC12-SC14) although there are still doubts about the length and am-
 123 plitude of the next solar cycle.

125 The current study is motivated by the correlation observed between the HMF in-
 126 tensity and the modulation of GCRs reported by Rahmanifard et al. (2020) and Schwadron
 127 et al. (2014). After a brief discussion of the modulation potential (Section 2), in Section
 128 3, we show that plotting these correlations for the past 24 cycles suggests we have moved
 129 to a modern secular minimum. In section 4, we investigate these correlation plots and
 130 categorize the observed trends to develop a tool to predict the subsequent cycles. Based
 131 on these trends, we show that SC25 will be as weak as or weaker than SC24. Through-
 132 out this paper, where we mention weaker (stronger) cycles, it refers to cycles with lower
 133 (higher) maximum HMF intensities than their previous cycles. Due to the well-established
 134 correlation between the sunspot number and HMF intensity, this can be roughly trans-
 135 lated to weaker/stronger sunspot numbers, as well. In section 5, we compare the pre-
 136 vious secular minima to SC21-24 to gain more insight into how the next few solar cy-
 137 cles might proceed. A brief discussion and concluding remarks are provided in section
 138 6 and section 7.

139 2 Modulation of the GCRs in the Heliosphere

140 The flux of GCRs is presumed to be constant within the nearby interstellar medium
 141 on the timescales that we consider. However, recent studies provide more evidence that
 142 our solar system might be in the boundary region between interstellar clouds (Linsky
 143 et al., 2019). Passage of the solar system through a cloud with a 10-fold enhancement
 144 in the density with respect to the LISM will shrink the heliosphere by a factor of one-
 145 fourth (Zank & Frisch, 1999). This increases the flux of GCRs at 1 AU by 2 - 100 times
 146 for energetic protons between 10^3 - 10^2 MeV (Scherer et al., 2002). The solar wind pres-
 147 sure dropping due to successive weak cycles can also participate in the shrinkage of the
 148 heliosphere, leading to less effective modulation of the GCRs (Schwadron et al., 2011).
 149 Additionally, the large magnetic structures that filter GCRs at the edge of the heliosphere
 150 are accumulated over several solar cycles. Therefore, we expect this filtration to change
 151 with long-term solar variations (See Rahmanifard et al., 2020, for further discussion).

152 Inside the heliosphere, GCRs interact with the HMF across multiple scales. Hence,
 153 changes in the modulation of GCRs over the course of multiple cycles provide valuable
 154 information about the state of the heliosphere and reveal an underlying effect that would
 155 be difficult to ascertain by other means. This modulation, which is closely related to the
 156 HMF and thus solar activity as discussed in Section 1, is prone to the inherent random-
 157 ness of solar activity. The effect of turbulent convection in the dispersion of the BMRs
 158 tilt, which is responsible for the birth of poloidal fields that initiate the next cycle, in-
 159 troduces randomness to the solar activity cycles and thus generates uncertainties in this
 160 analysis, which is based on the modulation of GCRs by the HMF.

161 The modulation of GCRs can be quantified by the so-called modulation potential
 162 adopted from the force field approximation of the Parker equation. The Badhwar-O'Neill
 163 2014 model, hereafter BON14, provides a simplified version of the problem by solving
 164 stationary Fokker-Plank equations to transport the local interstellar spectrum of GCRs
 165 to 1 AU (O'Neill et al., 2015). The modulation potential, also known as the solar mod-
 166 ulation parameter and deceleration potential, has a somewhat vague definition in the lit-
 167 erature since it was first introduced by Gleeson and Axford (1968). It is defined as a quan-

168 tity that approximately corresponds to the energy lost by GCR particles traveling from
 169 the LISM to the inner heliosphere and is related to the momentum per charge of the par-
 170 ticles penetrating through the heliosphere. In the BON14 model, however, the modu-
 171 lation potential (ϕ) is an input parameter, which presents the level of modulation within
 172 their choice of parameters. Therefore, its absolute value is not significant; its variation
 173 with time is of greater importance. BON14 incorporates an $\sim 8 - 14$ months delay through
 174 a function to find ϕ from sunspot number. In this way, they provide a time series of the
 175 modulation potential that extends back to 1750.

176 There are a few other models to find the intensity of GCRs, including Nymmik's
 177 model (Nymmik et al., 1996), which is a semi-empirical model similar to the BON14 model.
 178 Both these models describe GCR modulation through the heliosphere and thus provide
 179 invaluable knowledge about the structure of the heliosphere. BON2014 and Nymmik's
 180 model results are within 10% of each other, on average (Matthiä et al., 2013; de Wet,
 181 Slaba, Rahmanifard, Wislon, et al., 2020). Models similar to BON14 and Nymmik's model
 182 are appropriate for this type of analysis since they are based on the global sampling of
 183 GCRs calibrated to measurements near 1 AU. Alternatively, GCR fluxes can be used to
 184 find the characteristic modulation potential. CRaTER (Cosmic Ray Telescope for the
 185 Effect of Radiation, Spence et al., 2010) aims to investigate the radiation environment
 186 close to the lunar surface. The CRaTER instrument is designed to measure dose rates
 187 created by SEPs (solar energetic particles), GCRs, and other forms of radiation of lu-
 188 nar origin. de Wet, Slaba, Rahmanifard, Wilson, et al. (2020) used the Monte Carlo N-
 189 Particle 6 (MCNP6) transport code to create a response function between the modula-
 190 tion potential values and CRaTER-observed dose rates from GCRs. They used various
 191 boundary condition fluxes associated with specific values of modulation potential to pro-
 192 vide a modulation potential data set based on the dose rates observed by the most shielded
 193 pair of detectors with a triple coincidence condition (de Wet, Slaba, Rahmanifard, Wil-
 194 son, et al., 2020).

195 In our previous publication (Rahmanifard et al., 2020), we used CRaTER modu-
 196 lation potential data to investigate the correlation between the modulation potential and
 197 solar parameters for SC24. We adopted this method from Schwadron et al. (2014) to find
 198 a linear correlation between $\langle \phi \rangle / \langle V \rangle$ and $\langle B \rangle$ in logarithmic space, where
 199 ϕ is the modulation potential from CRaTER data, V is the solar wind speed, and B is
 200 the magnitude of the HMF intensity. The $\langle \rangle$ symbol represents moving averages ap-
 201 plied to data to eliminate the high-frequency variations and significant outliers (see Sec-
 202 tion 3 for more details). These studies were inspired by the power-law relation found by
 203 Schwadron et al. (2012) between the modulation potential (from Advanced Composition
 204 Explorer, ACE, data) and HMF, compatible with the slab turbulence of cosmic ray dif-
 205 fusion (le Roux et al., 1999).

206 The relationship between the modulation potential and the solar wind parameters
 207 has been examined in previous studies (Wibberenz & Cane, 2000; Wibberenz et al., 2002;
 208 Belov, 2000; Belov et al., 2001). Belov et al. (2001) used a contribution of several solar
 209 and heliospheric parameters including the current sheet tilt, polarity changes, and so-
 210 lar wind characteristics (the product of V_{SW} and $|B_{HMF}|$) in a semi-empirical model to
 211 predict GCR variations. They used this semi-empirical method to best describe the be-
 212 havior of 10 GV GCRs intensity during SC20-SC22. The temporal variations of GCRs
 213 intensity at high energies can be described by propagating disturbance in the forcefield
 214 approximation and a continuous recovery process (Chih & Lee, 1986; Wibberenz et al.,
 215 1998; Wibberenz & Cane, 2000). Wibberenz et al. (2002) used this approximation to de-
 216 scribe the GCRs depression as a function of $(V(t)/V_0)(B(t)/B_0)^n$ and used the observed
 217 intensity of GCRs for SC20-SC23 to show that $n \sim 1 - 2$ successfully predicts varia-
 218 tions in GCRs intensity. Several other studies have found the value for n to be close to
 219 2, which agrees well with equation A6 from Schwadron et al. (2014) (le Roux et al., 1999;
 220 Zank et al., 1998; Burger et al., 2000). Schwadron et al. (2014) reported a correlation

221 between modulation potential from ACE and CRaTER data, solar wind speed, and HMF
 222 intensity based on this equation. We updated this correlation for the entire cycle 24 to
 223 investigate the radiation environment in the coming solar cycle assuming a modern sec-
 224 ular minimum (Rahmanifard et al., 2020). While the modulation potential from CRaTER
 225 (de Wet, Slaba, Rahmanifard, Wilson, et al., 2020) only covers SC24, this type of anal-
 226 ysis can be extended to previous solar cycles using the BON14 modulation potential time
 227 series.

228 3 Correlation Plots Suggesting a Modern Secular Minimum

229 The hysteresis behavior observed for SC24 (Rahmanifard et al., 2020) motivated
 230 us to further investigate the correlation between the modulation potential from the BON14
 231 model and solar wind parameters. Looking at these correlations reveals trends that can
 232 potentially be used to deduce the longer-term behavior of the Sun. Sunspot numbers are
 233 available for the last 24 cycles in monthly resolution, which makes possible the recon-
 234 struction of solar parameters and modulation potential for these cycles. We used HMF
 235 intensities from Rahmanifard et al. (2017) (for SC1-24, in monthly resolution where 7-
 236 month moving averages were applied), and the solar wind speed from Owens et al. (2017)
 237 (in yearly resolutions for < 1973 and monthly resolution from 1973 onward with 7-month
 238 moving averages applied). For SC24, we used the most updated modulation values (monthly
 239 resolution) from CRaTER data (de Wet, Slaba, Rahmanifard, Wilson, et al., 2020), where
 240 they have applied 180-day moving averages. For SC1-23, we used the modulation param-
 241 eter from BON14 (O'Neill et al., 2015) (in monthly values). We applied moving aver-
 242 ages to the HMF strength and solar wind speed to eliminate the high-frequency varia-
 243 tions and significant outliers so that the underlying patterns and trends could become
 244 visible. Modulation potential values from BON14 are smooth enough so that applying
 245 moving averages does not make any significant differences.

246 Adopting a color code to differentiate secular variations through the last 24 cycles
 247 reveals an interesting trend (Figure 1). Using light blue for cycles associated with pre-
 248 vious secular minima (the Dalton, SC5-SC7 and the Gleissberg, SC12-SC14) and pink
 249 for all other cycles, which are mostly associated with secular maxima, creates two zones
 250 on the correlation plot. As can be seen, SC23 (red circles) falls in the secular maxima
 251 zone, as do the other cycles of the space age. However, the second half of SC23 moves
 252 toward the secular minima zone with a prolonged minimum connecting it to SC24. SC24,
 253 on the other hand, falls completely in the secular minima zone.

254 A pattern of a steep increase in the first half and a gentle decrease in the second
 255 half (most specifically in the last quarter) of SC24 seems to suggest another prolonged
 256 solar minimum leading to a weak SC25. Based on the correlation diagrams from the Dal-
 257 ton and the Gleissberg era (light blue circles), we expect SC25 and SC26 to stay in the
 258 secular minima zone and demonstrate activity levels below the average. Note that SC15
 259 and SC16 (pink circles overlapping the blue minima) came at the end of the Gleissberg
 260 era and had lower than average solar activity. Additionally, while ϕ values vary with B,
 261 for the same value of B, ϕ values are different, depending on how weak or strong the cy-
 262 cles are. This creates two zones on the correlation plot that can distinguish cycles as-
 263 sociated with secular minima from those associated with secular maxima.

264 4 Trends Observed in Previous Cycles

265 A closer look at previous cycles' correlation diagrams reveals trends that could be
 266 used to predict the subsequent cycles. In Figure 1, SC23 and SC24 demonstrate a steep
 267 increase in the first half and a gentle decrease in the second half, which might indicate
 268 a prolonged minimum and a weaker next cycle. Investigating these diagrams for the pre-
 269 vious 24 solar cycles (Figure 2 and Figure 3) shows that these trends are observed through
 270 the past secular minima as well (see Section 5).

271 Investigating these diagrams for the past 24 solar cycles shows the converse trend
 272 also exists, where a gentle increase in the first half and a steep decrease in the second
 273 half is indicative of a stronger subsequent cycle (similar to SC7 in Figure 2). In addi-
 274 tion, there are other possible forms, without as pronounced differences in the slopes be-
 275 tween the two halves, leaving the next cycle inconclusive. These diagrams are presented
 276 in Figure 2, where Panel (a) shows odd cycles and Panel (b) shows even cycles. In this
 277 figure, the first (second) half of each cycle is shown with green (blue) data point. This
 278 makes it easy to see the sequence of time in these hysteretic diagrams.

279 The shapes of the correlation diagrams are different for odd and even cycles (Fig-
 280 ure 2). After the magnetic field reversal in the solar maximum of even cycles ($A > 0$),
 281 the outward field lines in the northern pole cause positively charged ions such as GCR
 282 protons to drift down the poles. Therefore, these positive ions do not encounter irreg-
 283 ularities in the current sheet or CMEs, which enhances their flux in the third quarter
 284 of even cycles and broadens their peak. Conversely, in odd cycles ($A < 0$), ions travel
 285 into the heliosphere along the current sheet, where irregularities convect them out (for
 286 example see Jokipii & Thomas, 1981; Webber & Lockwood, 1988). This leads to the dis-
 287 tinctive alternate broad and sharp peaks in the flux of the GCRs, which in our corre-
 288 lation diagrams translate to hysteretic shapes for even cycles.

289 For odd cycles (Figure 2), it is quite straightforward to decide if a diagram is in-
 290 dicative of a weaker or stronger next cycle. If the first half of the cycle (green data points)
 291 falls below or more to the right (e.g. SC5), it can be indicative of a weaker next cycle
 292 and makes the shape of the diagram look like \swarrow . If the first half of odd cycles locates
 293 above or more to the left of the second half (blue data points), it can be indicative of
 294 a stronger next cycle (e.g. SC7) and has this shape \nearrow . For some of the cycles, this can
 295 be easily seen from the diagrams. However, for some other cycles, it can be very diffi-
 296 cult to distinguish these trends since the two halves fall roughly on top of one another
 297 (\asymp). For these cycles (e.g. SC9), we can consider the diagram to be inconclusive.

298 We further developed a method to distinguish which half is located on the top of
 299 the other and to separate cycles that are inconclusive. To this end, we found the line cor-
 300 related to the full solar cycle and defined the distance between the data points in the two
 301 halves in the space that is perpendicular to this correlated line (dashed black lines in Fig-
 302 ure 2). For each data point in the first half, the length of these dashed black lines shows
 303 the distance from the second half. If the second half is on the top ($(\langle \phi_2 \rangle / \langle V_2 \rangle$
 304 $) > (\langle \phi_1 \rangle / \langle V_1 \rangle)$), this value is multiplied by -1.0 . We found the averaged dis-
 305 tance between the two halves for each cycle by averaging over all these values for all the
 306 data points in the first half, for which the dashed line intersects with the second half.
 307 If this averaged value is positive, the first half is on the top for most of the cycle, and
 308 we expect the next cycle to be stronger (SC1 and SC7). If this value is negative, the first
 309 half is on the bottom, and we expect the next cycle to be weaker (SC3, SC5, SC11, SC13,
 310 SC19, and SC23). If this value is close to zero (for cycles 9, 15, 17, 21, the average of the
 311 distances are one order of magnitude smaller than the rest of the cycles), the next cy-
 312 cle remains inconclusive. Looking at the shape of these diagrams confirms the conclu-
 313 sions based on the numerical method. These averaged distances are gathered in Table
 314 1. Diagrams associated with odd cycles are shown in Figure 2. Furthermore, the years
 315 of each solar cycle and our prediction for the next cycle are provided in Figure 2.

316 The enhancement of GCR's flux in the second half of even cycles, which translates
 317 to an abrupt decrease in modulation values, results in the distinctive hysteretic shape
 318 of even cycles. Therefore, in even cycles, the second half (blue data points) always falls
 319 on the right (below) of the correlation diagrams, which makes it challenging to find trends
 320 to predict the next cycle for them. To come up with a method to categorize the corre-
 321 lation diagrams, we used the criteria that if the loop is relatively open, like SC8 (\nearrow),
 322 we consider this a cycle indicating a stronger next cycle. To decide if the shape of a di-
 323 agram is open, we find the averaged distance between the two halves for each cycle 1)

324 for the start of the cycle, 10% of the data points \bar{D}_{start} , shown in Figure 3 with solid
 325 red lines, and 2) for the full cycle (\bar{D}_{full}), dashed black lines. If the ratio $\bar{D}_{start}/\bar{D}_{full}$
 326 is greater than 0.5, it means the diagram shape is relatively open, and we can consider
 327 the cycle to predict a stronger next cycle. These values are provided in Table 2, and the
 328 shape of the diagrams are shown in Figure 3. Based on these values and the diagrams
 329 from Figure 3, we expect SC2, SC8, SC14, SC16, SC18, and SC22 to predict a stronger
 330 next cycle.

331 However, for SC12, SC20, and SC24, while this ratio is significantly greater than
 332 0.5, we can see from the shape of the diagrams that the cycle is definitely closed. This
 333 is because the tail of the second half after closing the cycle has extended in a way that
 334 the distance between the two halves is significant in comparison with the averaged dis-
 335 tance for the full cycles (see Figure 3). In these cases, we trust that we can see the cy-
 336 cle is closed, and we consider them as closed cycles. If solar cycles with closed diagrams
 337 further extend their tail towards smaller $\langle B \rangle$ values so that the data points are well
 338 passed the closing point (\mathcal{A}), this can be indicative of a prolonged solar minimum and
 339 predict a weaker next cycle. To find these cycles, we obtained the ratio between the length
 340 of the tail (second half data points with $\langle B \rangle$ smaller than the minimum $\langle B \rangle$ value
 341 for the first half data points) and the length of the full cycle (These values are provided
 342 in Table 2). SC4, SC20, and SC24 present a length ratio greater than 0.2 and thus pre-
 343 dict a weaker next cycle. The remaining cycles (SC6, SC10, SC12) present a length ra-
 344 tio close to zero (\mathcal{A} , see Table 2) and thus are considered inconclusive about the next
 345 cycle. We have provided years of solar cycles and our predictions for even cycles in Fig-
 346 ure 3.

347 Our predictions for both odd and even cycles are listed in Table 3. As can be seen
 348 in this table, among the 16 cycles for which the shape of diagrams is conclusive, we can
 349 successfully predict whether the next cycle is stronger or weaker for 13 cycles. SC23 shows
 350 that SC24 would be a weaker cycle, which agrees with our observations. SC24 is also pre-
 351 dicting the next cycle will be a weaker cycle (Figure 3). If this will be the case, we are
 352 probably entering an era of extreme decline in solar activity, similar to the Dalton and
 353 Gleissberg period.

354 Another look at the shapes presented in Table 3 might suggest that in most cases
 355 what dictates if the next cycle would be stronger (or weaker) than the current cycle is
 356 whether the cycle starts at lower (or higher) B values than it ends. This might be as-
 357 sociated with a correlation between the strength of solar cycles and the minimum B val-
 358 ues at the end of their previous cycles. This correlation has been previously examined
 359 in several studies (in terms of the SSN or polar magnetic field), for example, Brown (1976);
 360 Wilson (1990); Solanki et al. (2002); R. Cameron and Schussler (2007); Du et al. (2008);
 361 Vaquero and Trigo (2008); Kane (2008); Muñoz-Jaramillo et al. (2013); Yoshida (2014).
 362 We have shown this correlation in Figure 4, by presenting B_{Min} observed at the end of
 363 each cycle versus the B_{Max} associated with the next cycle (based on reconstructed val-
 364 ues of the HMF intensity from Rahmanifard et al., 2017). The black line in this figure
 365 shows the correlation with a correlation coefficient of 0.74 and a p-value of 0.00005. The
 366 gray shaded area shows the uncertainty region at 95% confidence interval. While data
 367 points are shown with grey circles, blue (or red) “x” signs mark cycles that are predicted
 368 to be weaker (or stronger) than their previous cycles based on Table 3. Blue squares (or
 369 green triangles) enclose gray circles for cycles associated with the Dalton (or Gleissberg)
 370 period.

371 As can be seen in Figure 4, cycles that are predicted to be weaker (gray circles with
 372 blue x) are mostly concentrated below the correlation line, cycles that are predicted to
 373 be stronger (gray circles with red x) have concentrated above the correlation line, and
 374 cycles that remain inconclusive (gray circles) are the most aligned with the correlation
 375 fit. Hence, excluding the data points associated with a weaker or stronger next cycle im-
 376 proves the correlation coefficient significantly ($R = 0.95$ and a $p = 0.0009$). This sug-

377 gests that on top of the well-established correlation between B_{Min} and cycle strength,
 378 our analysis provides additional information for predicting cycle strength. This additional
 379 information is probably reliant on the steps that connects the GCRs modulation to so-
 380 lar activity.

381 The HMF values used in this study are obtained from Rahmanifard et al. (2017)
 382 model. This model provides a historical record for HMF values using timescales asso-
 383 ciated with the processes involved in the balance of the heliospheric magnetic flux. It
 384 also uses sunspot numbers as a proxy for the closed magnetic flux introduced to this bal-
 385 ance throughout the previous 24 cycles. This model presents fairly good agreement with
 386 geomagnetic data as well as OMNI data. However, there are still differences between this
 387 model predictions and OMNI data, particularly in extrema. We have added datapoints
 388 from OMNI data (green circles with error bars, showing 95% confidence interval) to Fig-
 389 ure 4 to show that in spite of differences they still agree within uncertainties.

390 Using $B_{Min} = 3.98$ nT, obtained for May 2020 from Rahmanifard et al. (2017)
 391 model, we find SC25 B_{Max} to be $\sim 5.74 \pm 0.80$ (shown with a yellow star), which is sim-
 392 ilar to SC24 ($B_{Max} = 5.77$ nT). This makes these two cycles the weakest since SC14
 393 ($B_{Max} = 5.47$ nT). Using $B_{Min} = 4.18 \pm 0.03$ nT from OMNI data (yellow circle with
 394 95% confidence error bar) obtains $\sim 6.10 \pm 0.91$ for B_{Max} , which agrees with the pre-
 395 diction obtained based on Rahmanifard et al. (2017) model results within uncertainties.
 396 The predicted intensity of $B_{Max} = 5.74 \pm 0.80$ nT, or the 6.10 ± 0.91 value based on
 397 OMNI data, for SC25, is consistent with the amplitude of 95 to 130 averaged daily sunspot
 398 number as the consensus statement reported by the Solar Cycle 25 Prediction Panel

399 (<https://www.weather.gov/news/190504-sun-activity-in-solar-cycle>). Moreover, it
 400 would constitute an SC25 slightly weaker than SC13 ($B_{Max} = 6.14$ nT) in the Gleiss-
 401 berg era, although still stronger than SC6 ($B_{Max} = 4.72$ nT) in the Dalton era. While
 402 both these values present below-average solar activity, it must be noted that based on
 403 the trends found in this study they likely overestimate the strength on SC25.

404 5 Previous Secular Minima vs. a Modern Secular Minimum

405 Looking at correlation diagrams associated with the Dalton and the Gleissberg min-
 406 ima provides more insight into how the next few solar cycles might proceed. The Dal-
 407 ton minimum period covered SC5-SC7 (1790-1830), and it contains the weakest recorded
 408 solar activity since routine monthly sunspot numbers became available. In Figure 5a,
 409 we show SC4 to SC8 to demonstrate how cycles move to and from the secular minima
 410 zone. We have shown each cycle with a different color, with the beginning of each cy-
 411 cle being the darkest and the end of the cycle being the lightest. As can be seen, a shal-
 412 low slope in the last quarter of SC4 (green data points) leads to a weak SC5 (red). The
 413 same trend persists for SC5 (red) leading to a weak SC6. The shape of SC6 (blue) re-
 414 mains inconclusive (based on the trends introduced in Table 3) and leads to a SC7(grey)
 415 which contains higher B. Finally, SC7 breaks the trend by showing a steep slope in its
 416 last quarter, leading to a stronger SC8 (purple), ending the secular minimum.

417 The next secular minimum, the Gleissberg period (SC12-SC14), is shown in Fig-
 418 ure 5b. In this figure, we again applied different colors for each cycle, with the darkest
 419 data point denoting the beginning and the lightest denoting the end of cycles. The same
 420 trend—though not as pronounced as in the Dalton period—of a gradual decrease in $\langle \phi \rangle$
 421 / $\langle V \rangle$ in the last phases of these cycles leads to weak cycles one after another to
 422 form a secular minimum.

423 In Figure 5c, we show SC24 to compare it with the Dalton and Gleissberg cycles
 424 presented in panels a and b. While the shape of the correlation diagram is inconclusive
 425 for SC21 and SC22, a gradual decrease at the end of SC23 leads SC24 to reside in the

426 secular minima zone. SC23 shows that SC24 would be a weaker cycle, which agrees with
 427 our observations. SC24 is also predicting the next cycle will be a weaker cycle.

428 The last data points of SC24 (associated with May 2020, in light blue) represent
 429 modulation potential values below the predicted floor by the BON14 model, which likely
 430 is indicative of the start of SC25 (for further explanations see Rahmanifard et al., 2020).
 431 This is in agreement with (Leamon et al., 2020), who estimated the onset of SC25 would
 432 be in May 2020, $-1.5 +4$ months. However, Leamon et al. (2020) used a method based
 433 on terminator events (McIntosh et al., 2019) and predicted that SC25 will be significantly
 434 stronger than SC23 and SC24, which is contrast with our prediction of SC25. Starting
 435 from the observed point for May 2020, using a weighted average over the previous sec-
 436 ular minima cycles for the slope and using $B_{Max} = 5.74 \pm 0.80$ nT from Figure 4, we
 437 found a predicted linear correlation for SC25, grey solid line with grey dashed lines pre-
 438 senting the uncertainty region in Figure 5c. This uncertainty region represents our pre-
 439 dicted SC25, $-1.5 +4$ months uncertainty for the onset of SC25 along with our predicted
 440 uncertainty for SC25 B_{Max} . A more prolonged solar minimum will likely result in fur-
 441 ther decrease in B_{Min} at the end of SC24 resulting in a weaker SC25.

442 The prediction of $B_{Max} = 5.74 \pm 0.80$ nT from Figure 4 demonstrates an SC25
 443 slightly weaker than SC13 ($B_{Max} = 6.14$ nT) in the Gleissberg era, although still stronger
 444 than SC6 ($B_{Max} = 4.72$ nT) in the Dalton era. However, it is important to note that
 445 based on the trends found in this study the B_{Max} value used here likely overestimates
 446 the strength on SC25 (Section 4). The correlation plots and the radiation environment
 447 resulting from a Gleissberg-like and a Dalton-like SC25 were investigated in Rahmanifard
 448 et al. (2020). In a future study, we will investigate the radiation environment based on
 449 the correlation predicted here (Figure 5c).

450 6 Discussion

451 Correlations between the modulation potential values, solar wind speed, and the
 452 intensity of the HMF presented in this paper suggest that we are within a secular min-
 453 imum, and are further used to deduce trends to predict solar activity. The obtained cor-
 454 relation diagrams and any further conclusions based on their shapes are obviously re-
 455 liant on the accuracy of the inferred parameters employed in this study.

456 In Figure 1, we showed that plotting all the correlation diagrams in the last 24 so-
 457 lar cycles creates two distinctive zones associated with secular minima and maxima. Fur-
 458 thermore, we can see that in the last 23 solar cycles these diagrams have shifted to the
 459 secular minima zone only twice (the Dalton and the Gleissberg minima) and once more
 460 in the beginning of SC24. This suggests that we are currently in a secular minimum sim-
 461 ilar to the Dalton and the Gleissberg minima. This also means that the observed decline
 462 in solar activity will likely persist for another two solar cycles since both Dalton and Gleiss-
 463 berg minima were at least three solar cycles long. Therefore, we expect to see SC25 and
 464 SC26 stay in the secular minima zone and exhibit activity levels below the average.

465 Trends reported in this paper provide a way to predict the next solar cycle dur-
 466 ing the last phases of the current cycle. We showed that a steep increase in the first half
 467 and a gentle decrease in the second half of the correlation diagrams presented here can
 468 be indicative of a prolonged minimum leading to a weaker next cycle, while the oppo-
 469 site trend indicates the next cycle stronger than the current cycle. Based on the corre-
 470 lation presented in Figure 4 between the maximum HMF intensity of a cycle (B_{Max}) and
 471 the minimum HMF observed for the previous cycle (B_{Min}), we found that cycles that
 472 are predicted to be weaker (based on the trends found here) mostly demonstrate values
 473 lower than predicted by this correlation and cycles that are predicted to be stronger present
 474 larger values. This suggests that the correlation diagrams reveal a physical effect in ad-
 475 dition to the correlation between B_{Min} and B_{Max} . Although odd cycles have historically

476 shown to be stronger than their adjacent even cycles (Gnevyshev & Ohl, 1948), the small
 477 slope at the end of SC24 suggests that SC25 will be a weaker cycle than SC24. There-
 478 fore, while, based on Figure 4, SC25 is predicted to be as weak as SC24 with $B_{Max} =$
 479 5.74 ± 0.80 , this value likely overestimates the strength of SC25.

480 The correlation diagrams correctly predict thirteen cycles out of the sixteen cycles
 481 for which these trends have been observed. This means that in $\sim 70\%$ of cycles, where
 482 a prediction is possible, it correctly predicts whether the subsequent cycle will be weaker
 483 or stronger in $\sim 81\%$ of the cases. The seven cycles (30%) that remain inconclusive man-
 484 ifest a significant correlation between the maximum HMF intensity and the minimum
 485 HMF observed for the previous cycle. Therefore, the diagrams presented in this study
 486 along with the B_{Min} vs. B_{Max} correlation for the inconclusive cycles form a tool to pre-
 487 dict the strength of the next solar cycle at the end of the current cycle.

488 The modern secular minimum that we are experiencing will substantially affect our
 489 space radiation environment, and therefore future space missions. During the weak cy-
 490 cles that are awaiting us, solar maximum is safer for long-term space exploration due to
 491 more effective modulation of GCRs, provided that very large SEP events are infrequent.
 492 While SEP events are expected to be more frequent during solar maximum, a weak SC25
 493 as predicted in this study will make such events scarcer than before. However, to pro-
 494 tect the crew against radiation hazards caused by events such as the September 2017 event
 495 (Schwadron et al., 2018), real-time monitoring of solar events would be essential. The
 496 effect of these new conditions on the lunar radiation environment and explorations is yet
 497 to be understood (Looper et al., 2013; Spence et al., 2013).

498 A modern secular minimum would provide an exceptional opportunity to investi-
 499 gate our interstellar environment in the absence of extreme solar events. These years of
 500 unprecedently low solar activity provide a rare chance to study components of the inter-
 501 stellar medium that enter the heliosphere such as GCRs, the interstellar neutrals, and
 502 energetic neutral atoms with the interstellar origin. IBEX (Interstellar Boundary Ex-
 503 plorer, (McComas et al., 2009) measurements have already provided valuable data through
 504 SC24. Selected for launch in 2024, IMAP (Interstellar Mapping and Acceleration Probe,
 505 McComas et al., 2018) will further investigate the interaction between the heliosphere
 506 and the very local interstellar medium.

507 7 Conclusion

508 A persistent decline of the solar activity level, at the end of the space age secular
 509 maximum, indicates the possibility that the Sun has already entered a secular solar min-
 510 imum. In this paper, we used the correlation between the modulation potential and so-
 511 lar wind parameters to show that indeed we are in a secular minimum. We used trends
 512 observed in the correlation diagrams of the last 24 solar cycles to find a way to predict
 513 subsequent solar cycle during the last phases of the current cycle. Using this method,
 514 we predict SC25 to be as weak as or weaker than SC24 ($B_{Max} = 5.74 \pm 0.80$). Based
 515 on the historical records, if the Sun repeats the same trends observed for the Dalton and
 516 Gleissberg secular minima, we expect SC26 to be weak.

517 Acknowledgments

518 This work was supported by NASA SSERVI LEADER (grant number 80NSSC20M0021)
 519 and CRaTER, LRO program (contract number NNG11PA03C). All datasets are avail-
 520 able at <https://crater-web.sr.unh.edu/Rahmanifard2021>.

521 References

522 Abreu, J. A., Beer, J., Steinhilber, F., Tobias, S. M., & Weiss, N. O. (2008, oct). For

523 how long will the current grand maximum of solar activity persist? *Geophysical*
 524 *Research Letters*, 35(20). doi: 10.1029/2008GL035442

525 Babcock, H. W. (1961). The Topology of the Sun's Magnetic Field and the 22-
 526 Year Cycle. *Astrophysical Journal*, 133, 572. Retrieved from <http://adsabs.harvard.edu/doi/10.1086/147060>

527 Barnard, L., Lockwood, M., Hapgood, M. A., Owens, M. J., Davis, C. J., & Stein-
 528 hilber, F. (2011). Predicting space climate change. *Geophysical Research*
 529 *Letters*, 38(16), 7–12. doi: 10.1029/2011GL048489

530 Beer, J., McCracken, K. G., Abreu, J., Heikkilä, U., & Steinhilber, F. (2011). Cos-
 531 mogenic radionuclides as an extension of the neutron monitor era into the
 532 past: Potential and limitations. *Space Science Reviews*, 176(1-4), 89–100. doi:
 533 10.1007/s11214-011-9843-3

534 Belov, A. (2000). Large Scale Modulation: View from the Earth. In K. R. Bieber
 535 J.W., Eroshenko E., Evenson P., Flückiger E.O. (Ed.), *Cosmic rays and earth*
 536 (pp. 79–105). Dordrecht: Springer. doi: 10.1007/978-94-017-1187-6-5

537 Belov, A., Gushchina, R., Obrikko, V., Shelting, B., & Yanke, V. (2001). Interna-
 538 tional Conference on Cosmic Rays. In *Long-term variations of galactic cosmic*
 539 *rays and their relation to the solar magnetic field parameters* (pp. 3911–3914).
 540 Hamburg, Germany. Retrieved from <http://adsabs.harvard.edu/pdf/2001ICRC...10.3911B>

541 Bhowmik, P., & Nandy, D. (2018, dec). Prediction of the strength and timing of
 542 sunspot cycle 25 reveal decadal-scale space environmental conditions. *Nature*
 543 *Communications*, 9(1). doi: 10.1038/s41467-018-07690-0

544 Brown, G. M. (1976). What determines sunspot maximum? *Monthly Notices of the*
 545 *Royal Astronomical Society*, 174, 185–189. doi: 10.1093/mnras/174.1.185

546 Burger, R. A., Potgieter, M. S., & Heber, B. (2000). Rigidity dependence of cosmic
 547 ray proton latitudinal gradients measured by the Ulysses spacecraft' Impli-
 548 cations for the diffusion tensor. *Journal of Geophysical Research*, 105(27),
 549 447–455. doi: <https://doi.org/10.1029/2000JA000153>

550 Cameron, R., & Schussler, M. (2007). Solar Cycle Prediction Using Precursors and
 551 Flux Transport Models. *The Astrophysical Journal*, 659(1), 801–811. doi: 10
 552 .1086/512049

553 Cameron, R. H., Jiang, J., & Schussler, M. (2016, apr). Solar cycle 25: another
 554 moderate cycle? *Astrophysical Journal Letters*, 823(22), 5. Retrieved
 555 from <http://arxiv.org/abs/1604.05405> <http://dx.doi.org/10.3847/2041-8205/823/2/L22> doi: 10.3847/2041-8205/823/2/
 556 L22

557 Charbonneau, P. (2010). Dynamo Models of the Solar Cycle. *Living Reviews in So-*
 558 *lar Physics*, 2(1), 1–83. doi: 10.12942/lrsp-2005-2

559 Chih, P. P., & Lee, M. A. (1986). A perturbation approach to cosmic ray transients
 560 in interplanetary space. *Journal of Geophysical Research*, 91(A3), 2903–2913.
 561 doi: 10.1029/ja091ia03p02903

562 de Wet, W. C., Slaba, T. C., Rahmaniard, F., Wilson, J. K., Jordan, A. P.,
 563 Townsend, L. W., ... Spence, H. E. (2020). CRaTER observations and per-
 564 missible mission duration for human operations in deep space. *Life Sciences in*
 565 *Space Research*, 26(December 2019), 149–162. doi: 10.1016/j.lssr.2020.04.004

566 de Wet, W. C., Slaba, T. C., Rahmaniard, F., Wislon, J. K., Jordan, A. P.,
 567 Townsend, L. W., ... Spence, H. E. (2020). CRaTER Observed Permissi-
 568 ble Mission Duration for Human Operations in Deep Space. *Life Sciences in*
 569 *Space Research*, 26, 149–162. Retrieved from <https://www.sciencedirect.com/science/article/pii/S2214552420300341?via%3Dihub> doi:
 570 10.1016/j.lssr.2020.04.004

571 Du, Z. L., Wang, H. N., & Zhang, L. Y. (2008). A running average method for pre-
 572 dicting the size and length of a solar cycle. *Chinese Journal of Astronomy and*

578 *Astrophysics*, 8(4), 477–488. doi: 10.1088/1009-9271/8/4/12

579 Gleeson, L. J., & Axford, W. I. (1968, dec). Solar Modulation of Galactic Cosmic

580 Rays. *The Astrophysical Journal*, 154, 1011. doi: 10.1086/149822

581 Gnevyshev, M., & Ohl, A. (1948). On the 22-year cycle of solar activity. *Astron.*

582 *Zh.*, 25, 18–20.

583 Hathaway, D. H. (2010). The Solar Cycle Imprint / Terms of Use. *Living Reviews in*

584 *Solar Physics*, 7(1), 1–65. Retrieved from <http://adsabs.harvard.edu/abs/2010LRSP....7....1H>

585 Hazra, S., & Nandy, D. (2019). The origin of parity changes in the solar cycle. *Monthly Notices of the Royal Astronomical Society*, 489(3), 4329–4337. doi: 10.1093/mnras/stz2476

586 Hazra, S., Passos, D., & Nandy, D. (2014). A stochastically forced time delay solar

587 dynamo model: Self-consistent recovery from a maunder-like grand minimum

588 necessitates a mean-field alpha effect. *Astrophysical Journal*, 789(1). doi:

589 10.1088/0004-637X/789/1/5

590 Jiang, J., Wang, J. X., Jiao, Q. R., & Cao, J. B. (2018, aug). Predictability of the

591 Solar Cycle Over One Cycle. *The Astrophysical Journal*, 863(2), 159. doi: 10.3847/1538-4357/aad197

592 Jokipii, J. R., & Thomas, B. (1981). EFFECTS OF DRIFT ON THE TRANS-

593 PORT OF COSMIC RAYS IV. MODULATION BY A WAVY INTERPLAN-

594 ETARY CURRENT SHEET J. *The Astrophysical Journal*, 243, 1115–1122.

595 Retrieved from https://books.google.be/books?id=dzyy3X1mUSOC&dq=physiologie+humaine+herve+\{e\}+gu\{e\}nard\&hl=fr\&sa=X\&ved=0ahUKEwjplf_{m3sLziAhWEaFAKHUkiBEkQ6AEIKDAA

596 Kane, R. P. (2008). Prediction of solar cycle maximum using solar cycle lengths. *Solar*

597 *Physics*, 248(1), 203–209. doi: 10.1007/s11207-008-9125-8

598 Leamon, R. J., McIntosh, S. W., Chapman, S. C., & Watkins, N. W. (2020). Tim-

599 ing Terminators: Forecasting Sunspot Cycle 25 Onset. *Solar Physics*, 295(2),

600 1–18. doi: 10.1007/s11207-020-1595-3

601 Leighton, R. B. (1969). A Magneto-Kinematic Model of the Solar Cycle. *Astrophysical*

602 *Journal*, 156(April), 1. Retrieved from <http://adsabs.harvard.edu/doi/10.1086/149943>

603 le Roux, J. A., Zank, G. P., & Ptuskin, V. S. (1999, nov). An evaluation of per-

604 pendicular diffusion models regarding cosmic ray modulation on the basis of a

605 hydromagnetic description for solar wind turbulence. *Journal of Geophysical*

606 *Research: Space Physics*, 104(A11), 24845–24862. doi: 10.1029/1999ja900318

607 Linsky, J. L., Redfield, S., & Tilipman, D. (2019). The Interface Between The Outer

608 Heliosphere and The Inner Lism: Morphology of The Local Interstellar Cloud,

609 Its Hydrogen Hole, Stromgren Shells, and 60Fe Accretion. *arXiv*, 41. doi:

610 10.3847/1538-4357/ab498a

611 Lockwood, M. (2001). Long-term variations in the magnetic fields of the Sun and

612 the heliosphere: Their origin, effects, and implications. *Journal of Geophysical*

613 *Research: Space Physics*, 106(A8), 16021–16038. doi: 10.1029/2000ja000115

614 Lockwood, M. (2010). Solar change and climate: An update in the light of the cur-

615 rent exceptional solar minimum. *Proceedings of the Royal Society A: Mathe-*

616 *matical, Physical and Engineering Sciences*, 466(2114), 303–329. doi: 10.1098/rspa.2009.0519

617 Lockwood, M., Stamper, R., & Wild, M. N. (1999). A doubling of the Sun’s coronal

618 magnetic field during the past 100 years. *Nature*, 399(6735), 437–439. doi: 10.1038/20867

619 Looper, M. D., Mazur, J. E., Blake, J. B., Spence, H. E., Schwadron, N. A., Go-

620 lightly, M. J., ... Townsend, L. W. (2013). The radiation environment near

621 the lunar surface: CRaTER observations and Geant4 simulations. *Space*

622 *Weather*, 11(4), 142–152. doi: 10.1002/swe.20034

623 Matthiä, D., Berger, T., Mrigakshi, A. I., & Reitz, G. (2013). A ready-to-use galac-

624

tic cosmic ray model. *Advances in Space Research*, 51(3), 329–338. doi: 10.1016/j.asr.2012.09.022

McComas, D. J., Allegrini, F., Bochsler, P., Bzowski, M., Christian, E. R., Crew, G. B., ... Zank, G. P. (2009, nov). Global observations of the interstellar interaction from the Interstellar Boundary Explorer (IBEX). *Science*, 326(5955), 959–962. doi: 10.1126/science.1180906

McComas, D. J., Christian, E. R., Schwadron, N. A., Fox, N., Westlake, J., Allegrini, F., ... Zirnstein, E. J. (2018). Interstellar Mapping and Acceleration Probe (IMAP): A New NASA Mission. *Space Science Reviews*, 214(8), 116. Retrieved from <http://dx.doi.org/10.1007/s11214-018-0550-1> doi: 10.1007/s11214-018-0550-1

McIntosh, S. W., Chapman, S., Leamon, R. J., Egeland, R., & Watkins, N. W. (2020). Overlapping Magnetic Activity Cycles and the Sunspot Number: Forecasting Sunspot Cycle 25 Amplitude. *Solar Physics*, 295(12). Retrieved from <http://dx.doi.org/10.1007/s11207-020-01723-y> doi: 10.1007/s11207-020-01723-y

McIntosh, S. W., Leamon, R. J., Egeland, R., Dikpati, M., Fan, Y., & Rempel, M. (2019). What the Sudden Death of Solar Cycles Can Tell Us About the Nature of the Solar Interior. *Solar Physics*, 294(7). Retrieved from <http://dx.doi.org/10.1007/s11207-019-1474-y> doi: 10.1007/s11207-019-1474-y

Muñoz-Jaramillo, A., Dasi-Espuig, M., Balmaceda, L. A., & Deluca, E. E. (2013). Solar cycle propagation, memory, and prediction: Insights from a century of magnetic proxies. *Astrophysical Journal Letters*, 767(2). doi: 10.1088/2041-8205/767/2/L25

Nandy, D. (2021). Progress in Solar Cycle Predictions: Sunspot Cycles 24–25 in Perspective: Invited Review. *Solar Physics*, 296(3). Retrieved from <http://dx.doi.org/10.1007/s11207-021-01797-2> doi: 10.1007/s11207-021-01797-2

Nymmik, R. A., Panasyuk, M. I., & Suslov, A. A. (1996). No TitleGalactic cosmic ray flux simulation and prediction. *Advances in Space Research*, 17(2), 19–30. doi: [https://doi.org/10.1016/0273-1177\(95\)00508-C](https://doi.org/10.1016/0273-1177(95)00508-C).

O'Neill, P. M., Golge, S., & Slaba, T. C. (2015). *NASA-TP-2015-218569 - Badhwar-O'Neill 2014 Galactic Cosmic Ray Flux Model Description* (Tech. Rep. No. March). Houston: NASA Johnson Space Center. Retrieved from <https://ntrs.nasa.gov/search.jsp?R=20150003026>

Owens, M. J., Lockwood, M., Barnard, L., & Davis, C. J. (2011, oct). Solar cycle 24: Implications for energetic particles and long-term space climate change. *Geophysical Research Letters*, 38(19). doi: 10.1029/2011GL049328

Owens, M. J., Lockwood, M., & Riley, P. (2017). Global solar wind variations over the last four centuries. *Nature Publishing Group*, 7(January), 1–11. Retrieved from <http://dx.doi.org/10.1038/srep41548> doi: 10.1038/srep41548

Pal, S., Dash, S., & Nandy, D. (2020). Flux Erosion of Magnetic Clouds by Reconnection With the Sun's Open Flux. *Geophysical Research Letters*, 47(8), 1–10. Retrieved from <https://doi.org/10.1029/2019GL086372> doi: 10.1029/2019GL086372

Passos, D., Nandy, D., Hazra, S., & Lopes, I. (2014). A solar dynamo model driven by mean-field alpha and Babcock-Leighton sources: Fluctuations, grand-minima-maxima, and hemispheric asymmetry in sunspot cycles. *Astronomy and Astrophysics*, 563, 1–9. doi: 10.1051/0004-6361/201322635

Pesnell, W. D. (2012). Solar Cycle Predictions (Invited Review). *Solar Physics*, 281(1), 507–532. doi: 10.1007/s11207-012-9997-5

Pesnell, W. D. (2016). Predictions of Solar Cycle 24: How are we doing? *Space Weather*, 14(1), 10–21. doi: 10.1002/2015SW001304

Rahmanifard, F., de Wet, W. C., Schwadron, N. A., Owens, M. J., Jordan, A. P., Wilson, J. K., ... Townsend, L. W. (2020). Galactic Cosmic Radiation in the

688 Interplanetary Space Through a Modern Secular Minimum. *Space Weather*,
689 18(9). doi: 10.1029/2019SW002428

690 Rahmanifard, F., Schwadron, N. A., Smith, C. W., McCracken, K. G., Duderstadt,
691 K. A., Lugaz, N., & Goelzer, M. L. (2017, mar). Inferring the Heliospheric
692 Magnetic Field Back through Maunder Minimum. *The Astrophysical Journal*,
693 837(2), 165. doi: 10.3847/1538-4357/aa6191

694 Riley, P., Lionello, R., Linker, J. A., Cliver, E., Balogh, A., Beer, J., ... Koutchmy,
695 S. (2015). Inferring the Structure of the Solar Corona and Inner Heliosphere
696 During the Maunder Minimum Using Global Thermodynamic Magnetohy-
697 drodynamic Simulations. *The Astrophysical Journal*, 802(2), 105. Retrieved
698 from <http://stacks.iop.org/0004-637X/802/i=2/a=105?key=crossref>
699 .4f09aa5a229837dae1776cb700089919 doi: 10.1088/0004-637X/802/2/105

700 Scherer, K., Fichtner, H., & Stawicki, O. (2002). Shielded by the wind: The in-
701 fluence of the interstellar medium on the environment of Earth. *Journal of At-*
702 *mospheric and Solar-Terrestrial Physics*, 64(7), 795–804. doi: 10.1016/S1364-
703 -6826(02)00078-0

704 Schwadron, N. A., Baker, T., Blake, B., Case, A. W., Cooper, J. F., Golightly, M.,
705 ... Zeitlin, C. (2012). Lunar radiation environment and space weathering from
706 the Cosmic Ray Telescope for the Effects of Radiation (CRaTER). *Journal of*
707 *Geophysical Research E: Planets*, 117(3). doi: 10.1029/2011JE003978

708 Schwadron, N. A., Blake, J. B., Case, A. W., Joyce, C. J., Kasper, J., Mazur, J.,
709 ... Zeitlin, C. J. (2014). Special Section : Does the worsening galactic cos-
710 mic radiation environment observed by CRaTER preclude future manned
711 deep space exploration ? *Space Weather*, 12(11), 622–632. Retrieved from
712 <http://onlinelibrary.wiley.com/doi/10.1002/2014SW001084/full> doi:
713 10.1002/2014SW001084. Received

714 Schwadron, N. A., Connick, D. E., & Smith, C. W. (2010). MAGNETIC
715 FLUX BALANCE IN THE HELIOSPHERE. *The Astrophysical Journal*,
716 722(September), 132–136. Retrieved from <http://iopscience.iop.org/article/10.1088/2041-8205/722/2/L132/meta> doi: 10.1088/2041-8205/
717 722/2/L132

719 Schwadron, N. A., Rahmanifard, F., Wilson, J., & Jordan, A. P. (2018). Update
720 on the Worsening Particle Radiation Environment Observed by CRaTER and
721 Implications for Future Human Deep-Space Exploration. *Space Weather*, 16,
722 289–303.

723 Schwadron, N. A., Spence, H. E., & Came, R. (2011). Does the space environment
724 affect the ecosphere? *Eos*, 92(36), 297–298. doi: 10.1029/2011EO360001

725 Solanki, S. K., Schüssler, M., & Fligge, M. (2002). Secular variation of the Sun's
726 magnetic flux. *Astronomy and Astrophysics*, 383, 706. Retrieved from http://adsabs.harvard.edu/cgi-bin/nph-data{_}query?bibcode=2002A{\&}A..383..706S{\&}link{_}type=ABSTRACT{\%}5Cnpapers2://publication/doi/10.1051/0004-6361:20011790 doi: 10.1051/0004-6361:20011790

730 Spence, H. E., Case, A. W., Golightly, M. J., Heine, T., Larsen, B. A., Blake, J. B.,
731 ... Charara, Y. (2010, jan). CRaTER: The cosmic ray telescope for the effects
732 of radiation experiment on the lunar reconnaissance orbiter mission. *Space*
733 *Science Reviews*, 150(1-4), 243–284. doi: 10.1007/s11214-009-9584-8

734 Spence, H. E., Golightly, M. J., Joyce, C. J., Looper, M. D., Schwadron, N. A.,
735 Smith, S. S., ... Zeitlin, C. (2013). Relative contributions of galactic cosmic
736 rays and lunar proton "albedo" to dose and dose rates near the Moon. *Space*
737 *Weather*, 11(11), 643–650. doi: 10.1002/2013SW000995

738 Steinhilber, F., Abreu, J. A., & Beer, J. (2008). Solar modulation during the
739 Holocene. *Astrophysics and Space Sciences Transactions*, 4(1), 1–6. doi:
740 10.5194/astra-4-1-2008

741 Upton, L. A., & Hathaway, D. H. (2018, aug). An Updated Solar Cycle 25 Predic-
742 tion With AFT: The Modern Minimum. *Geophysical Research Letters*, 45(16),

743 8091–8095. doi: 10.1029/2018GL078387

744 Usoskin, I. G. (2013). A History of solar activity over millennia. *Living Reviews in*
 745 *Solar Physics*, 10(1), 1–88.

746 Vaquero, J. M. (2016). Long-term variation of solar activity: recent progress.
 747 In S. P.-H. S. Arribas, A. Alonso-Herrero, F. Figueras, C. Hernández-
 748 Monteagudo, A. Sánchez-Lavega (Ed.), *Scientific meeting of the spanish astro-*
 749 *nomical society*. Bilbao, Spain. Retrieved from www.sidc.be/silso/https://ui.adsabs.harvard.edu/abs/2017hsa9.conf..579V/abstract

750 Vaquero, J. M., & Trigo, R. M. (2008). Can the solar cycle amplitude be predicted
 751 using the preceding solar cycle length? *Solar Physics*, 250(1), 199–206. doi: 10
 752 .1007/s11207-008-9211-y

753 Wang, Y. M. (2017, sep). *Surface Flux Transport and the Evolution of the Sun's Po-*
 754 *lar Fields* (Vol. 210) (No. 1-4). Springer Netherlands. doi: 10.1007/s11214-016
 755 -0257-0

756 Webber, W. R., & Lockwood, J. A. (1988). Characteristics of the 22-year modu-
 757 lation of cosmic rays as seen by neutron monitors. *Journal of Geophysical Re-*
 758 *search*, 93(A8), 8735. doi: 10.1029/ja093ia08p08735

759 Weiss, N. O., & Tobias, S. M. (2016). Supermodulation of the Sun's magnetic activi-
 760 *ty: The effects of symmetry changes. Monthly Notices of the Royal Astronomi-*
 761 *cal Society*, 456(3), 2654–2661. doi: 10.1093/mnras/stv2769

762 Wibberenz, G., & Cane, H. V. (2000). Simple analytical solutions for propagating
 763 diffusive barriers and application to the 1974 minicycle. *Journal of Geophysical*
 764 *Research: Space Physics*, 105(A8), 18315–18325. doi: 10.1029/1999ja000457

765 Wibberenz, G., le Roux, J. A., & Potgieter, M. S. (1998). Transient Effects and
 766 Disturbed Conditions. *Space Science Reviews*, 83, 309–348. doi: 10.1023/A:
 767 1005083109827

768 Wibberenz, G., Richardson, I. G., & Cane, H. V. (2002). A simple concept
 769 for modeling cosmic ray modulation in the inner heliosphere during so-
 770 lar cycles 20–23. *Journal of Geophysical Research*, 107(A11), 1353. doi:
 771 10.1029/2002JA009461

772 Wilson, R. M. (1990). On the level of skill in predicting maximum sunspot number:
 773 A comparative study of single variate and bivariate precursor techniques. *Solar*
 774 *Physics*, 125(1), 143–155. doi: 10.1007/BF00154784

775 Yoshida, A. (2014, aug). Difference between even- and odd-numbered cycles in the
 776 predictability of solar activity and prediction of the amplitude of cycle 25. *An-*
 777 *nales Geophysicae*, 32(8), 1035–1042. doi: 10.5194/angeo-32-1035-2014

778 Zank, G. P., & Frisch, P. C. (1999, jul). Consequences of a Change in the Galac-
 779 *tic Environment of the Sun. The Astrophysical Journal*, 518, 965–973. doi: 10
 780 .1086/307320

781 Zank, G. P., Matthaeus, W. H., Bieber, J. W., & Moraal, H. (1998). The radial and
 782 latitudinal dependence of the cosmic ray diffusion tensor in the heliosphere.
 783 *Journal of Geophysical Research: Space Physics*, 103(A2), 2085–2097. doi:
 784 10.1029/97ja03013

Table 1: The Averaged Distance Between the Two Halves for Odd Cycles

Solar Cycle	Averaged distance	Next cycle will be
1	0.024	Stronger
3	-0.050	Weaker
5	-0.039	Weaker
7	0.043	Stronger
9	-0.005	Inconclusive
11	-0.032	Weaker
13	-0.013	Weaker
15	0.006	Inconclusive
17	0.004	Inconclusive
19	-0.017	Weaker
21	-0.004	Inconclusive
23	-0.024	Weaker

Table 2: How Closed the Shape of the Cycle Is

Solar Cycle	Distance ratio (Start / full cycle)	Diagram is	Length ratio (Tail / full cycle)	Next cycle will be
2	0.802	Open		Stronger
4	0.142	Closed	0.231	Weaker
6	0.067	Closed	0	Inconclusive
8	1.862	Open		Stronger
10	0.239	Closed	0	Inconclusive
12	1.059	Closed by eye	0.045	Inconclusive
14	1.284	Open		Stronger
16	0.904	Open		Stronger
18	1.280	Open		Stronger
20	1.613	Closed by eye	0.264	Weaker
22	0.844	Open		Stronger
24	0.764	Closed by eye	0.221	Weaker

Table 3: Predicting the Next Solar Cycle Based on the Correlation Diagrams

Trends Observed						
Cycle is	Odd	Even	Odd	Even	Odd	Even
Next cycle will be	Weaker	Weaker	Stronger	Stronger	Inconclusive	Inconclusive
Cycle Numbers	3, 5, 11, 13, 19, 23	4, 20, 24	1, 7	2, 8, 14 16, 18, 22	9, 15, 17 21	6, 10, 12,
Our prediction is correct (✓)/incorrect (X)	✓, ✓, ✓	✓, X, ?	✓, ✓	✓, X, ✓	✓, ✓, X	

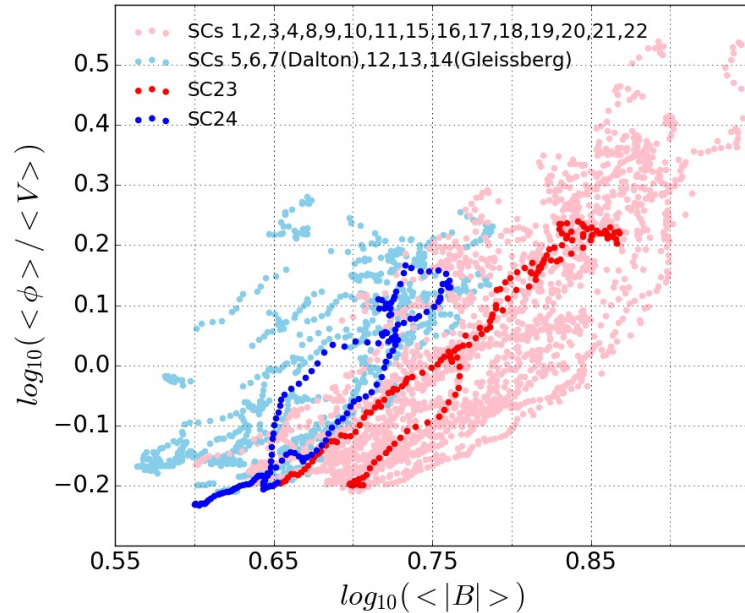


Figure 1: Correlation diagrams between $\langle \phi \rangle / \langle V \rangle$ and $\langle B \rangle$ are shown in logarithmic space for the previous 24 solar cycles for which sunspot data is available. Cycles associated with secular maxima (minima) are shown in pink (light blue). SC23 and SC24 are shown in red and blue. It can be seen that at the end of cycle 23 we transited from the secular maxima zone to the secular minima zone.

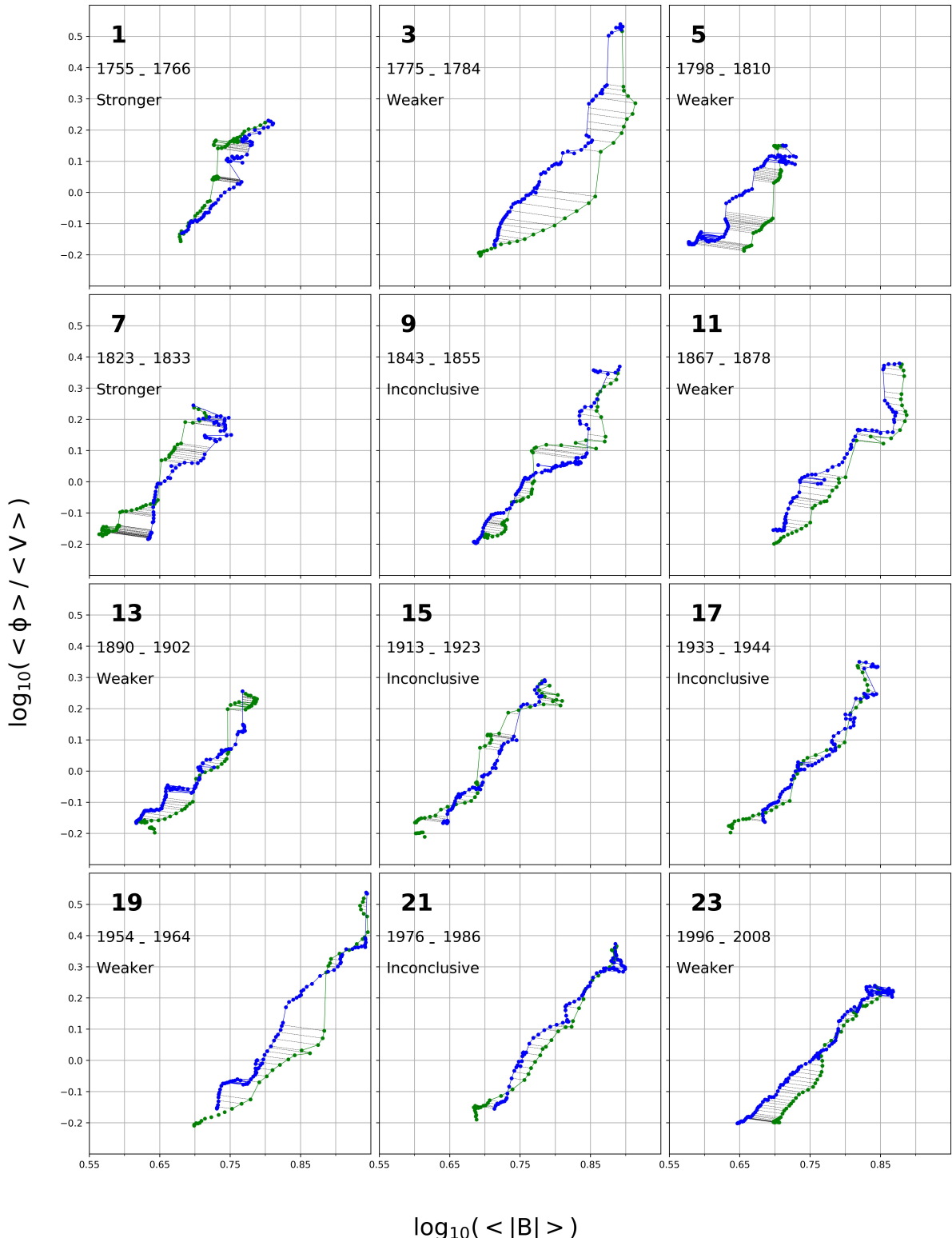


Figure 2: Correlation diagrams for odd cycles. Green data points represent the first half of cycles, and blue data points denote the second half of cycles. Dashed black lines that connect the two halves are used to find the distance between the two halves.

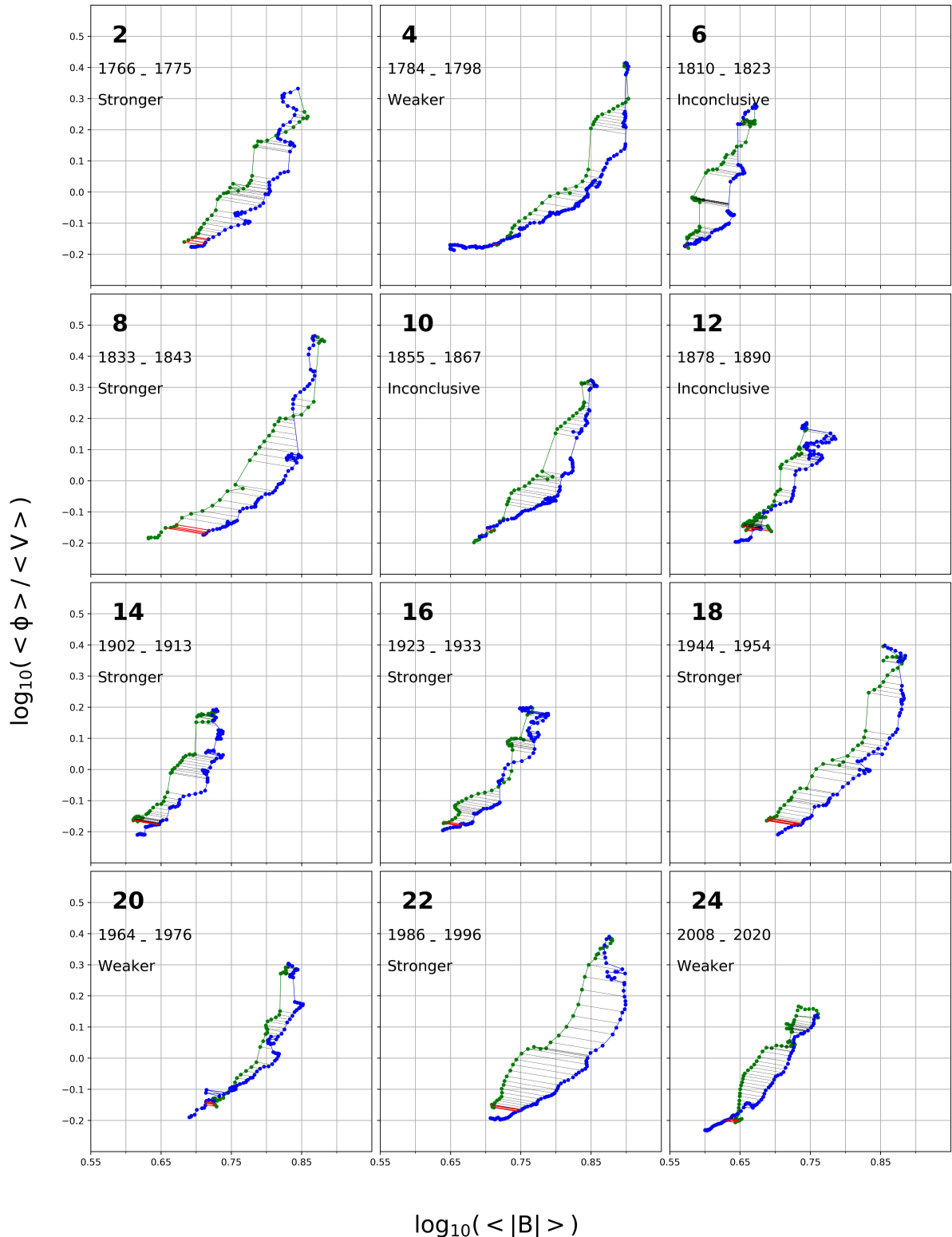


Figure 3: Correlation diagrams for even cycles. Green data points represent the first half of cycles, and blue data points denote the second half of cycles. Dashed black lines that connect the two halves are used to find the distance between the two halves. Red solid lines that connect the start of the two halves are used to determine if the cycle is open.

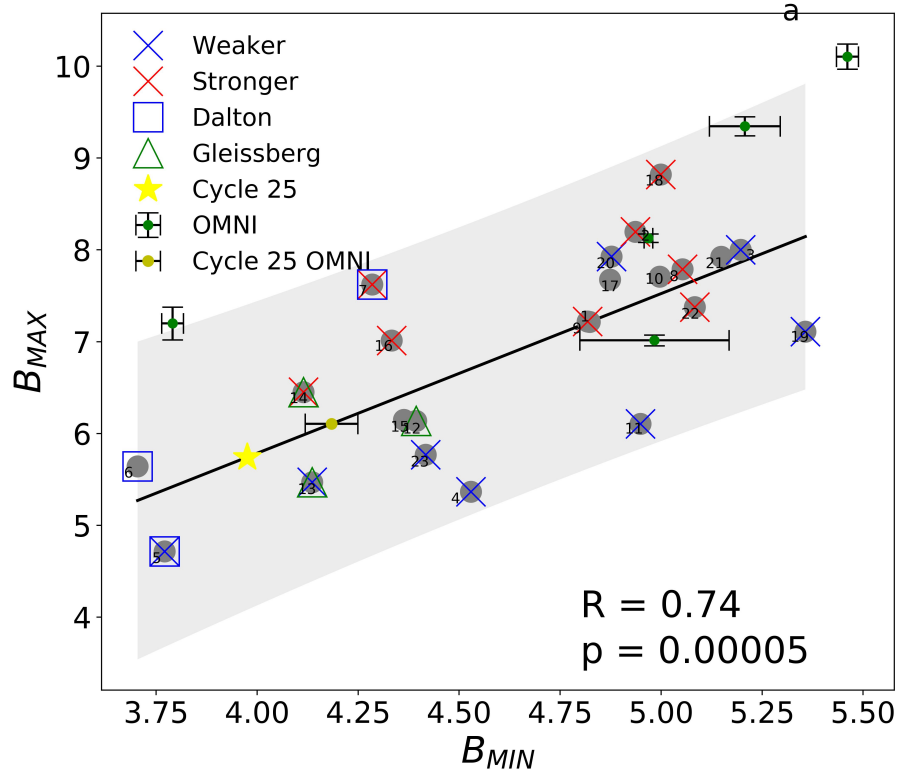


Figure 4: B_{Max} versus B_{Min} at the end of the previous cycle. The black line shows the correlation with a correlation coefficient of ~ 0.74 and a p-value of 0.00005. Gray shaded area represents uncertainty with 95% confidence level. Grey circles represent data points for each cycle, and blue (or red) x signs mark cycles that are predicted to be weaker (or stronger) than their previous cycles. Considering only the inconclusive cycles provides a better correlation ($R = 0.95$ and $p = 0.0009$). Blue (or green) squares (or triangles) enclose cycles associated with the Dalton (or Gleissberg) period. Green circles with error bars represent datapoints from the OMNI data set. The yellow star (circle with error bar) shows our prediction for SC25 based on SC24 B_{Min} from Rahmanifard (2017) (or OMNI data).

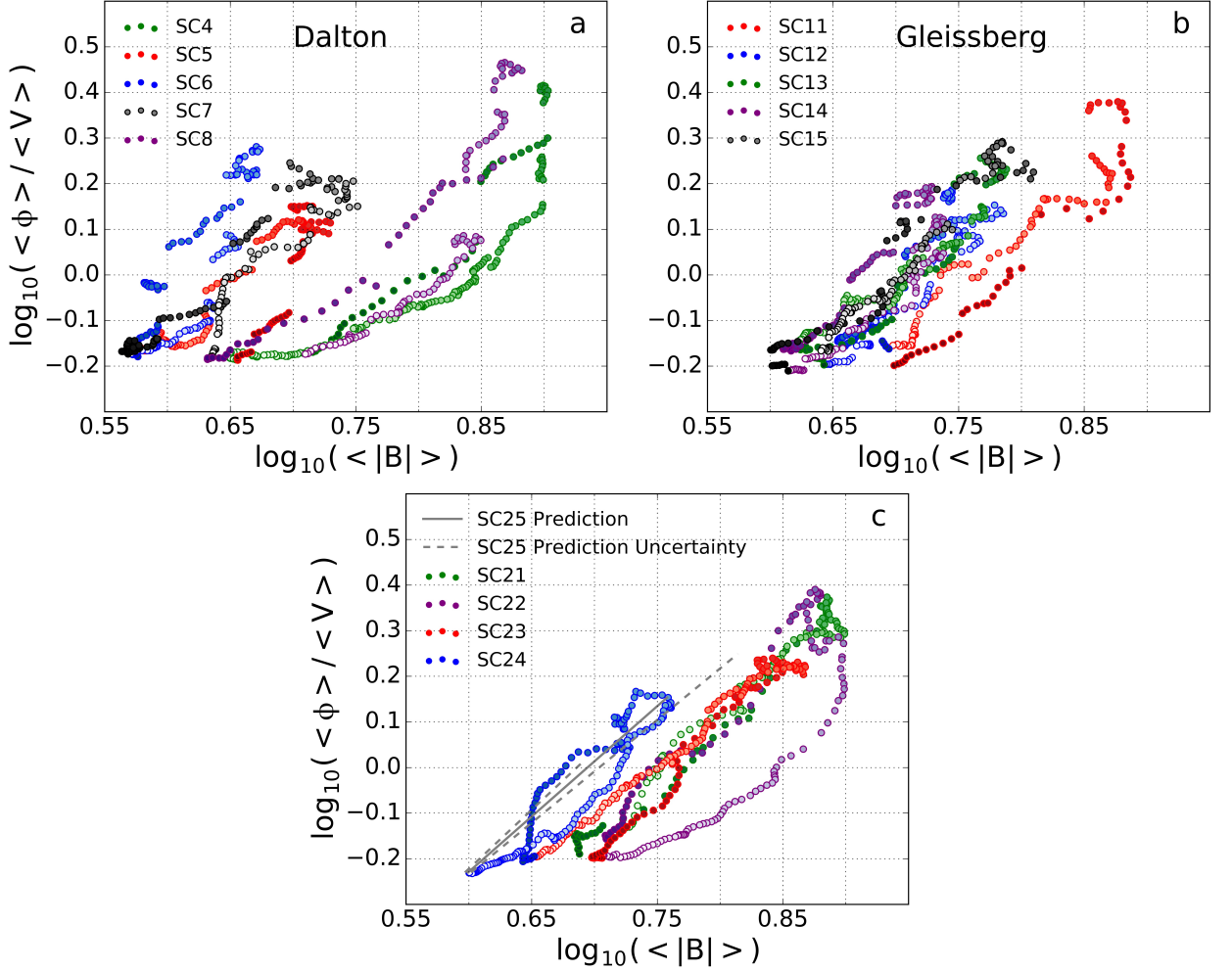


Figure 5: Panels a, b, and c show the correlation diagrams for the Dalton, the Gleissberg, and modern era. In panel a, in addition to SC5 to SC7, we have included SC4 and SC8 to show how the transit occurs to and from a secular minimum. In the same way, in panel b, we have shown the transit from SC11 to SC12 through SC15, for the Gleissberg period. In panel c, we have shown the SC21 through SC24, with SC24 seeming to be the first cycle of a modern secular/grand minimum. In panel c, in addition to SC21-SC24 our prediction for SC25 is shown based on a prediction of $B_{Max} = 5.74 \pm 0.80$ from panel a using grey solid line. Gray dashed lines represent uncertainty.